An Alternative Route to Molybdenum Disulfide Nanotubes

Wen Kuang Hsu,[†] Bao He Chang,[†] Yan Qiu Zhu,[†] Wei Qiang Han,[‡] Humberto Terrones,[§] Mauricio Terrones,[‡] Nicole Grobert,[†] Anthony K. Cheetham,[⊥] Harold W. Kroto,[†] and David R. M. Walton*[,†]

Contribution from the School of Chemistry, Physics and Environmental Science, University of Sussex, Brighton BN1 9QJ, U.K., Max-Planck-Institut für Metallforschung, Seestrasse 92, 70174 Stuttgart, Germany, Instituto de Física, UNAM, AP 1-1010, 76000, Querétaro, México, and Materials Research Laboratory, University of California, Santa Barbara, California 93106

Received May 10, 2000

Abstract: Molybdenum disulfide ($(MoS_2)_n$) nanotubes are generated when polycrystalline MoS_2 powder, covered by Mo foil, is heated to ca. 1300 °C in the presence of H_2S. Electron diffraction reveals the presence of zigzag arrangements within the tube walls.

Tenne et al. were the first to produce inorganic $(MoS_2)_n$ nanotubes[1−7] by reacting MoO_{3-x} with H_2S in the gas phase, a method similar to conventional chemical vapor deposition (CVD). In this approach, H_2S was passed over MoO_3, maintained at 800−900 °C, and the $(MoS_2)_n$ nanotubes, together with polyhedral particles, were collected from the rear of the reaction zone. The transformation of MoO_3 into a MoS_2 layered structure commences as S replaces O at the metal oxide surface. H_2S then diffuses through the outer layers via defects, gradually replacing O by S.[3,4] However, incomplete sulfur substitution may also result in encapsulated oxide particles during tube growth. The initial morphology of the MoO_3 material, however, exercises template control over the resulting fullerene-like $(MoS_2)_n$ nanostructures. Consequently, if MoO_3 precursors can be constructed in the shape of nanoparticles or whiskers before exposure to H_2S, the generation of $(MoS_2)_n$ nanotubes or nanoparticles will be more likely to occur, i.e., by the template effect. In this paper, we describe the generation of MoS_2 nanotubes with well-defined tube walls and free of encapsulated material, by heating MoS_2 powder in an H_2S/Ar atmosphere.

The apparatus consisted of a water-cooled stainless steel cylindrical chamber, 50 cm (height) × 45 cm (diameter), fitted with inlets connected to Ar and H_2S and an outlet to a vacuum pump. Two water-cooled stainless steel electrodes, ca. 5 cm apart and located at the center of the chamber, were connected to a Mo foil heating element (60 × 5 × 0.025 mm). MoS_2 powder (20 mg, <2 μm, 99% purity, Aldrich, UK) was sonicated with acetone (20 cm^3) for 5 min, and then a few drops of the mixture were deposited on the foil by means of a pipet. The acetone was allowed to evaporate so that the MoS_2 formed a thin layer, covering the upper surface of the Mo foil. A rectangular sheet (20 × 5 × 0.025 mm) of Mo foil, bent into a U-shaped cross section, acting as the collector, was placed above the MoS_2 film, in such way that only the edges of the foil were in contact with the film, the middle portion being ca. 4 mm above the film (Figure 1). The chamber was repeatedly evacuated and purged with Ar. Finally, it was filled with Ar (350 Torr) and H_2S (450 Torr). By setting the direct current at 30−35 A, the temperature of the lower flat Mo foil was raised to ca. 1200−1300 °C (optical pyrometry), while the upper U-shaped Mo foil attained ca. 600−800 °C. The current was maintained for ca. 30 min. After cooling to room temperature, the resulting dark soot-like product was removed from the upper Mo foil and dispersed in acetone. After 1 min of ultrasonic treatment, the dispersion was transferred to a Cu grid and coated with holey carbon film, and the acetone was allowed to evaporate. The residue was examined by transmission electron microscopy (Hitachi 7100 operating at 125 keV and JEOL 4000FX operating at 400 keV), energy dispersed X-ray analysis (EDX, NORAN instruments attached to the either microscope), and selective area electron diffraction.

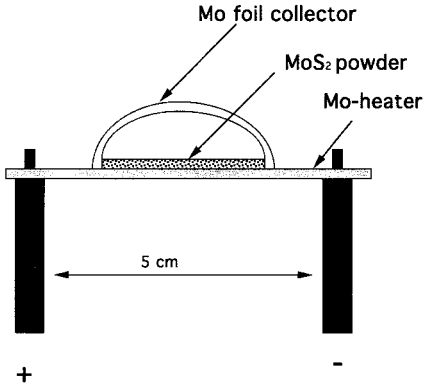

Figure 1. MoS_2 nanotube generation apparatus.

TEM (Figure 2a) and HRTEM (Fig 2b,c) revealed the presence of long, well-defined nanotubes (30−60 nm diameter,

[†] University of Sussex.
[‡] Max-Planck-Institut für Metallforschung.
[§] Instituto de Física, UNAM.
[⊥] University of California, Santa Barbara.

(1) Feldman, Y.; Wasserman, E.; Srolovitz, D. J.; Tenne, R. *Science* **1995**, *267*, 222.
(2) Srolovitz, D. J.; Safran, S. A.; Homyonfer, M.; Tenne, R. *Phys. Rev. Lett.* **1995**, *74*, 1779.
(3) Homyonfer, M.; Mastai, Y.; Hershfinkel, M.; Volterra, V.; Hutchison, J. L.; Tenne, R. *J. Am. Chem. Soc.* **1996**, *118*, 7804.
(4) Feldman, Y.; Frey, G. L.; Homyonfer, M.; Lyakhovitskaya, V.; Margulis, L.; Cohen, H.; Hodes, G.; Hutchison, G. L.; Tenne, R. *J. Am. Chem. Soc.* **1996**, *118*, 5362.
(5) Margulis, L.; Dluzewski, P.; Feldman, Y.; Tenne, R. *J. Microsc.* **1996**, *181*, 68.
(6) Frey, G. L.; Elani, S.; Homyonfer, M.; Feldman, Y.; Tenne, R. *Phys. Rev B* **1998**, *57*, 6666.
(7) Frey, G. L.; Tenne, R.; Matthews, M. J.; Dresselhaus, M. S.; Dresselhaus, G. *J. Mater. Res.* **1998**, *13*, 2412.

10.1021/ja001607i CCC: $19.00
Published on Web 09/27/2000

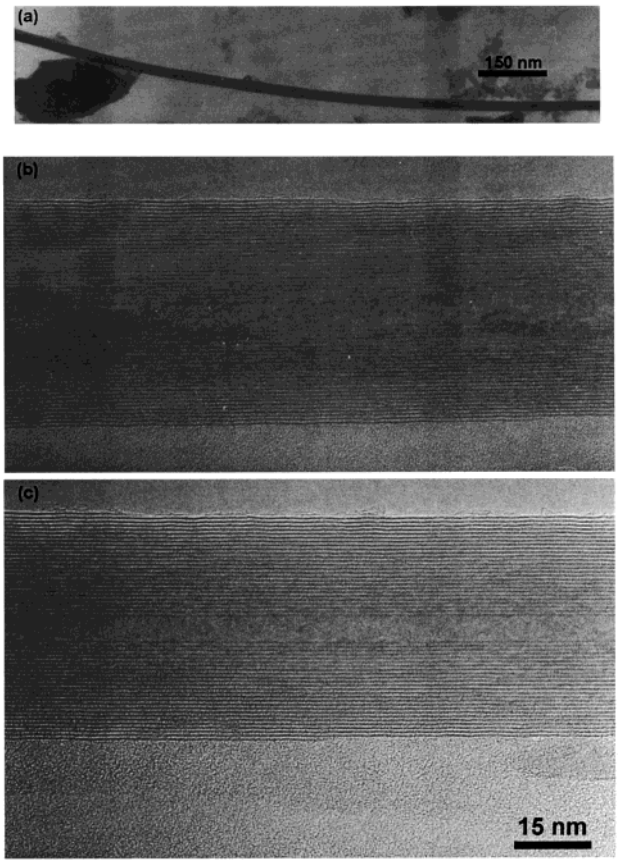

Figure 2. Low-resolution image of MoS_2 nanotube (a) and high-resolution (b,c) TEM images for MoS_2 nanotubes.

2−8 μm in length), together with crystalline MoS_2 flakes. The yield of the nanotubes is ca. 2−5%, based on TEM observation. The *d* spacing in the tube walls along the *c*-axis is ca. 6.2 Å, and the number of layers in the tube walls is ca. 20−40, significantly greater than that observed in previous reports (4−6 layers).[1,5] Interestingly, the variation of inner core diameters throughout the individual tubes appears to be quite limited. For example, the nanotube inner core diameters are ca. 7 nm in Figure 2b,c and do not vary significantly throughout the nanotubes observed here. We were unable to estimate the Mo/S ratio by EDX, due to overlap between the S and Mo peaks. However, the layered MoS_2 structure must have 1:2 stoichiometry.

For carbon nanotubes, the central core can be easily established when the image magnification is set at 10 000. As image magnification reaches 400 000 (JEOL 4000 FX, resolution 1.6 Å), the 3.4 Å *d* spacing along the *c*-axis can be distinguished. In MoS_2 nanotubes, the layered structure along the *c*-axis can be easily observed when the image magnification is set above 150 000, due to larger *d* spacing. Nevertheless, the inner core of the tubes becomes visible only when the image magnification exceeds 100 000 (as also found for WS_2 nanotubes).[8] According to Iijima's observations[9] on carbon nanotubes, TEM fringes are produced when 4 or 5 carbon atoms lie within a ca. 2-Å-thick wall, aligned with the electron beam. The TEM fringe contrast is denser in the parallel sections of the tube walls (i.e., more carbon atoms aligned to the electron beam) than in the vertical sections, which accounts for the observation of the discernible

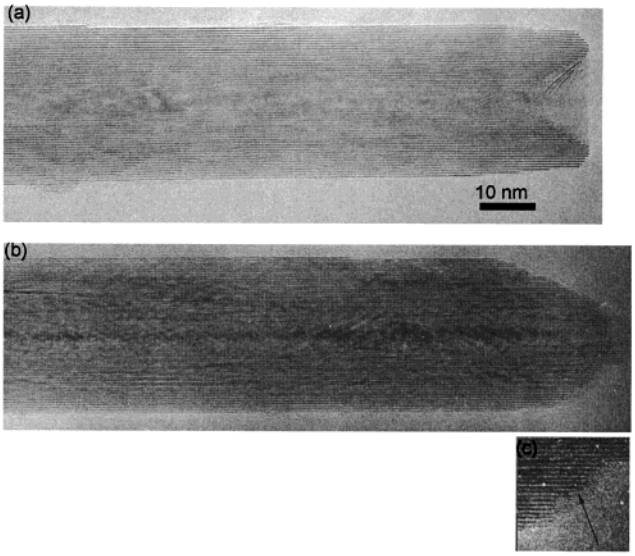

Figure 3. Open-ended MoS_2 nanotubes (a) inwardly triangularly shaped and (b) outwardly triangularly shaped. A folding structure is also present (c).

central cores for carbon nanotubes at low magnification. The indistinct central core of MoS_2 nanotubes at low magnification is possibly due to the strong scattering of the beam by Mo and S, so that the fringe contrast with the tube walls between the parallel and vertical sections is not easily differentiated.

We note that MoS_2 nanotubes, generated by heating MoS_2 and H_2S, are open-ended (Figure 3a,b). This outcome does not appear to result from mechanical damage (e.g., during sample dispersion in acetone by ultrasound). Open tube ends were also observed when the sample was dispersed by gentle shaking in acetone, without ultrasound treatment. HRTEM also revealed the presence of folded structures at the open tube ends (e.g., Figure 3b). Similar folding, or edge sealing, has been observed previously in carbon nanotubes.[10,11] However, the structure of the folded MoS_2 layers must differ from the graphite system and may involve the presence of additional $(MoS)_x$ units acting as dangling bond "sealer" units (Figure 3c). The morphology of the open tube ends is of two types: inward-cone (Figure 3a) or outward-cone (Figure 3b). The inner core diameter of the tubes remains unchanged at the open ends, and no amorphous materials were found trapped there. The larger *d* spacing (the van der Waals interaction is very weak) and open-ended structure may facilitate shifting and rotation of the MoS_2 shells, as suggested for carbon nanotubes.[12]

Electron diffraction measurements on individual $(MoS_2)_n$ nanotubes revealed the presence of zigzag and various helical arrangements. The electron diffraction pattern of a typical zigzag-edged tube, shown in Figure 4, is consistent with the simulated diffraction pattern (Figure 5a). The coexistence of nonhelical and helical structures was not observed for the individual MoS_2 nanotubes, which is surprising because it is not easy to see how a congruent orientation (namely, identical chirality) can be maintained in a concentric structure without varying the 6.2-Å *d* spacing.[13] A similar example is provided by carbon nanotubes, where variation of the *d* spacing along

(8) Zhu, Y. Q.; Hsu, W. K.; Grobert, N.; Chang, B. H.; Terrones, M.; Terrones, H.; Kroto, H. K.; Walton, D. R. M. *J. Chem. Mater*. **2000**, *12*, 1190.
(9) Iijima, S. *J. Cryst. Growth* **1980**, *50*, 675.
(10) Iijima, S.; Ajayan, P. M.; Ichihashi, T. *Phys. Rev.Lett*. **1992**, *69*, 3100.
(11) Sarkar, A.; Kroto, H. W.; Endo, M. *Carbon* **1995**, *33*, 51.
(12) Charlier, J.-C.; Michenaud, J.-P. *Phys. Rev. Lett*. **1993**, *70*, 1858.
(13) Hsu, W. K.; Firth, S.; Redlich, Ph.; Terrones, M.; Terrones, H.; Zhu, Y. Q.; Grobert, N.; Schilder, A.; Clark, R. J. H.; Kroto, H. W.; Walton, D. R. M. *J. Mater. Chem*. **2000**, *10*, 1425.

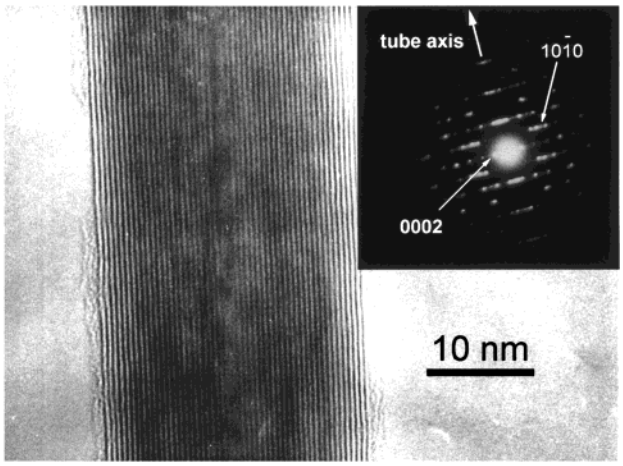

Figure 4. Electron diffraction of a single MoS_2 nanotube (middle) showing a zigzag diffraction pattern (top right), along the tube axis (white arrow), as consistent with a simulated diffraction pattern (top, Figure 5a).

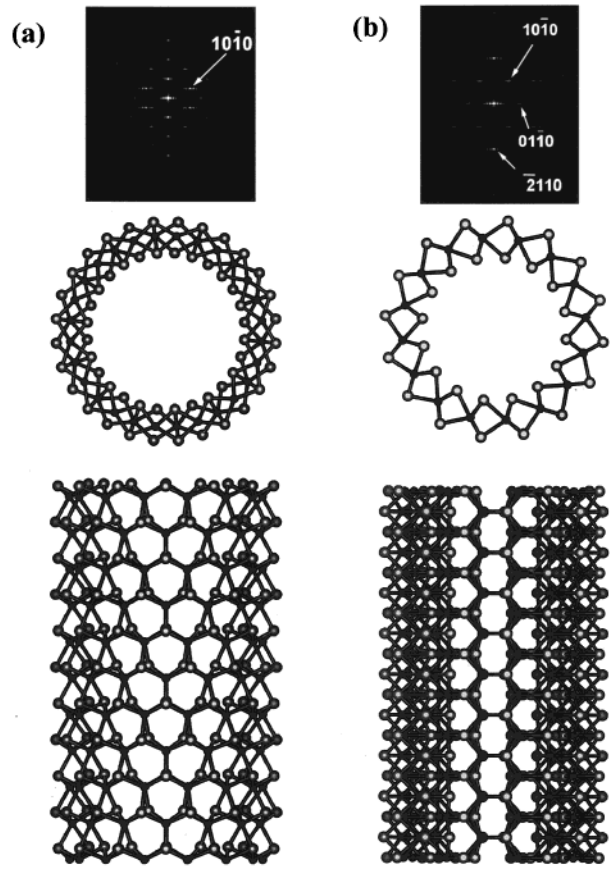

Figure 5. 5. (a) Zigzag simulated single-layer MoS_2 nanotube, viewed along the tube axis (middle) and the *c*-axis (lower), and simulated diffraction pattern of single zigzag sheet (top). (b) Armchair simulated single-layer MoS_2 nanotube, viewed along the tube axis (middle) and the *c*-axis (lower), and simulated diffraction pattern of single armchair sheet (top). Note that the zigzag and armchair structures in MoS_2 system are similar to the graphene sheet, in which the M−S bonds in a hexagonal-like rings are either in parallel (zigzag) or vertical (armchair) to the tube axis.

the *c*-axis has been observed.[14,15] In a $(MoS_2)_n$ nanotube, individual MoS_2 sheets consist of an alternating structure: a Mo layer sandwiched between two S layers (i.e., S−Mo−S,

(14) Liu, M.; Cowley, J. M. *Carbon* **1993**, *31*, 393.
(15) Liu, M.; Cowley, J. M. *Carbon* **1995**, *33*, 225.

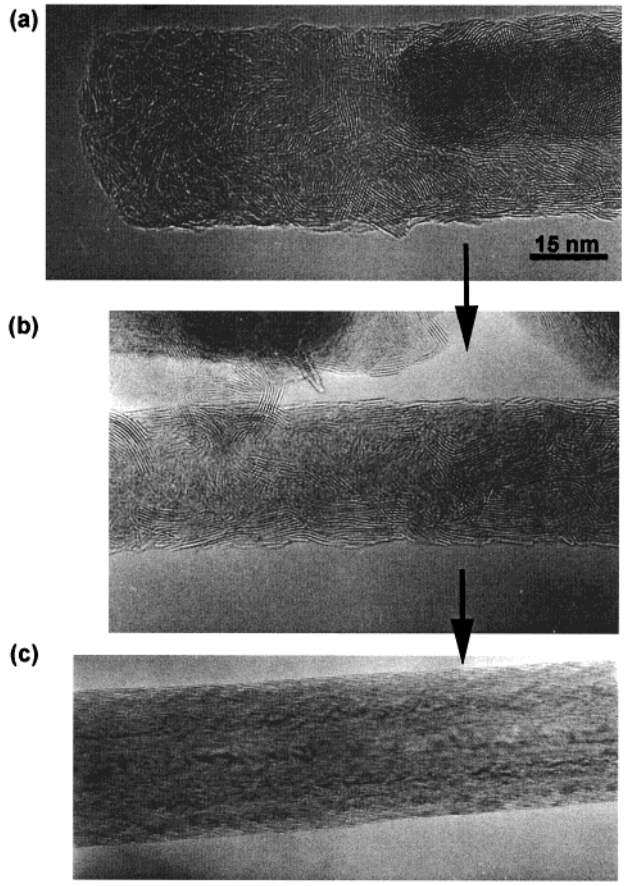

Figure 6. HRTEM images of MoS_2 (a) nanorod, (b) a similar structure, and (c) a complete nanotube.

see Figure 5a,b). Sulfur atoms bond to the metal, and there are no Mo−Mo or S−S bonds present. The concertina-like structure for $(MoS_2)_n$ nanotubes implies that the force constant for distorting a single $(MoS_2)_n$ tube and, in particular, stretching it should be significantly lower than the C−C stretching vibration. In this context, the marked regularity of layer stacking along the *c*-axis with identical chirality, as revealed by HRTEM and electron diffraction, may be due to this intrinsic flexibility of the MoS_2 sheets, because the variation in layer spacing as the tube walls thicken can be easily accommodated. It has been shown that carbon nanotubes can be bent reversibly, accompanied by buckling,[16,17] due to the high flexibility of graphite sheets. Large-angle carbon nanotube bending (e.g., >90°), however, does lead to tube collapse, i.e., kink formation.[18] However, depending on the tube diameter and the number of shells, the critical angles for switching from tube buckling to kinking is quite variable. The mechanical properties of MoS_2 nanotubes remain to be evaluated. Nevertheless, transformation of tube buckling to kink formation may require larger deformations than in the case of carbon nanotubes. Figure 5a,b shows simulated zigzag and armchair $(MoS_2)_n$ nanotubes, respectively, together with associated diffraction patterns. Two features are observed in Figures 5a,b. First, S atoms are more compacted in the inner layer than the outer, as viewed along the tube axis (Figure 5a,b, middle). Second, the configuration of the armchair tube, as viewed along the tube axis (Figure 5b, middle), has a

(16) Falvo, M. R.; Clary, G. L.; Talyor, R. M., II; Chl, V.; Brooks, F. P., Jr.; Washburn, S.; Superfine, R. *Nature* **1997**, *389*, 582.
(17) Lourie, O.; Cox, D. M.; Wagner, H. D. *Phys. Phys B* **1998**, *81*, 1638.
(18) Iijima, S. *J. Chem. Phys*. **1996**, *104*, 2089.

higher degree of flexibility than the zigzag and should be more elastic than the zigzag tube along the *c*-axis.

Some very peculiar $(MoS_2)_n$ nanorods were also found in the product (Figure 6a). These rods are composed of domains of short-range layered arrays, arranged in a fairly chaotic fashion. Interestingly, a similar nanorod, with discernible inner core and tube wall structure, was also found (Figure 6b). An insight into a possible formation mechanism may be established for MoS_2 nanotubes upon heating, by monitoring observable infrastructures, both rod (Figure 6a) and tube (Figure 6c).

Several conclusions are clear: (a) Oxide particles were not involved in the $(MoS_2)_n$ nanotube growth. (b) Nanotubes were not produced when a Mo foil, with no MoS_2 covering, was heated at 1300 °C in the presence of H_2S. This result indicates that the Mo foil (heater) did not directly participate in the growth of $(MoS_2)_n$ nanotubes. In other words, the source of Mo is mainly the MoS_2 powder. (c) H_2S decomposed during the reaction, as indicated by the appearance of a pasty yellow deposit on the inner wall of the reactor, concentrated specifically in the region directly above the heater. Thus, transient atomic S or small S clusters are likely to be present, which react with Mo. (d) When H_2S was replaced by H_2, $(MoS_2)_n$ nanotubes were not produced. (e) When MoS_2 powder was replaced by MoO_3 or Mo, nanotubes were not generated. (f) $(MoS_2)_n$ nanotubes did not grow on the surface of the heated Mo foil, in the absence of the Mo foil collector. MoS_2 nanotube formation must therefore involve the chemical vapor-phase transport of a volatile molybdenum species from the hotter to the cooler foil.[19] We propose that hot Mo reacts with H_2S to form volatile MoS_3, which subsequently decomposes to MoS_2 and S on the collector. MoS_2 is rod-shaped (e.g., Figure 6a) due to the temperature gradient, vertical to the Mo foil. These nanorods are continuously subjected to annealing and gradually become more ordered (Figure 6b), so that a complete tube structure is eventually formed (Figure 6c). As a result, lengthening and thickening of the tube walls occur simultaneously, which accounts for tube walls of identical chirality (i.e., zigzag). The formation of open-ended MoS_2 nanotubes is likely to have occurred, based on the proposed mechanism. First, all MoS_2 layers are formed at the same time within a tube. The formation of curved structures, which is responsible for the tube cap generation, is therefore relatively disfavored during annealing, as compared with the tube body generation. Accordingly, the excess MoS_2 units at the tube ends do not form the tube cap but contribute to the extension of tube length. Second, the dangling bonds at the open-ended tubes can be satisfied by the presence of a small number of MoS_2 units (inset, Figure 3b) without involving significant curvature. Second, if the MoS_2 shells are helically arranged within a tube, the preferential generation of cone-shaped structures at the open-ended tubes is likely.[20]

Acknowledgment. We thank EPSRC (W.K.H.), Royal Society (B.H.C., N.G.), the Japan Fine Ceramic Centre (Y.Q.Z.), the DGAPA-UNAM, Sabbatical scheme (108199), and CONACYT (25237-E and J31192-U) (H.T., M.T.), Mexico, for financial support, C.N.R. Rao for helpful discussions, and J. Thorpe and D. Randall (Sussex) for providing valuable assistance with the electron microscope experiment.

JA001607I

(19) Lenz, M.; Gruehn, R. *Chem. Rev.* **1997**, *97*, 2967.

(20) Iijima, S. *Mater. Sci. Eng.* **1993**, *172*, B19.